Characterization of atomic motion governing grain boundary migration

Hao Zhang and David J. Srolovitz
Department of Mechanical and Aerospace Engineering, Princeton University, Princeton, New Jersey 08540, USA

Jack F. Douglas
Polymers Division and Center for Theoretical and Computational Materials Science, National Institute of Standards and Technology, Gaithersburg, Maryland 20899, USA

James A. Warren
Metallurgy Division and Center for Theoretical and Computational Materials Science, National Institute of Standards and Technology, 100 Bureau Drive, Stop 8554, Gaithersburg, Maryland 20899, USA
(Received 4 May 2006; published 11 September 2006)

Molecular dynamics simulations were employed to study atomic motion within stationary and migrating asymmetric tilt grain boundaries. We employ several measures of the "complexity" of the atomic trajectories, including the van Hove correlation function, the non-Gaussian parameter, and dynamic entropy. There are two key types of dynamical events within the grain boundaries (i) a stringlike cooperative motions parallel to the tilt axis and occurring on a characteristic time scale of $\approx$25 ps and (ii) atomic motion across the grain boundary plane occurring on a characteristic time scale of $\approx$150 ps. The characteristic times associated with each type of event decreases with increasing driving force for boundary migration. We present evidence as to how the driving force biases these types of events, leading to boundary migration. While the stringlike atomic motion is an intrinsic feature of grain boundary dynamics and is important for grain boundary migration, it is the second type of event that controls grain boundary migration rates.

DOI: 10.1103/PhysRevB.74.115404 PACS number(s): 61.72.Mm, 68.35.Ja

I. INTRODUCTION

Although the study of grain boundaries has been an active area of research for several decades, the basic mechanisms by which grain boundaries migrate have been largely unexplored. Many earlier studies have focused on grain boundary structure, grain boundary thermodynamics, and diffusion along grain boundaries. This is somewhat surprising given the importance of grain boundary migration (GBM) in the thermomechanical processing of polycrystalline materials. The connection between grain boundary structure, grain boundary dynamics, and grain boundary migration is intrinsically a question of the boundary migration mechanism. In the present study, we use molecular dynamics simulations to examine the internal dynamics of grain boundaries and how these change when the grain boundary migrates. This provides some important hints into the underlying mechanisms of boundary migration.

Ashby,[1] Bishop *et al.*[2] and, more recently, Cahn and Taylor[3] have suggested that grain boundary migration can also produce a coupled tangential motion between the two interacting grains. Migration implies motion of the grain boundary perpendicular to itself, without the need for the motion of the two grains parallel to the grain boundary. In a coupled tangential motion, the boundary migrates and the two grains move relative to one another in the direction parallel to the boundary plane. In particular Cahn and Taylor[3] postulate that, in the absence of grain boundary sliding, the component of the velocity of the two grains relative to each other parallel to the grain boundary, $v_{\parallel}$, is proportional to the grain boundary velocity (normal to itself), v_{n}. This coupling constant is a function of the misorientation between the two crystals. Recent molecular dynamics simulations[4] of the migration of a series of symmetric boundaries driven by an applied shear rate demonstrated that $v_{\parallel}/v_{\mathrm{n}}$ is indeed nonzero, as predicted by Cahn and Taylor.[3] Ashby,[1] using a bubble raft model, demonstrated that this ratio is also a function of the grain boundary inclination. While several theories have been proposed to describe grain boundary migration (see Refs. 5–11), our understanding of the basic atomic mechanisms associated with grain boundary migration remains rudimentary.

Our recent molecular dynamics simulations of the migration of asymmetric $\Sigma5$ [010] tilt (several different boundary inclinations) grain boundaries revealed how atoms move during grain boundary migration.[12] In those simulations, the migration of asymmetric boundaries is driven via the application of a biaxial stress (in the boundary plane) rather than an imposed fixed shear strain rate or shear stress.[4,11] Even in simulations where the boundary migrates in excess of 5 nm there are no significant shear displacements of the grains relative to each other.[12] Figure 1 shows the vector displacements of the atoms during the simulated migration of a $\Sigma5$ 36.9° [010] asymmetric tilt grain boundary. The atomic positions shown in this figure are those for the interpenetrated perfect crystal lattice sites for the two crystals (rotated with respect to each other by 36.9° about the [010] axis). As the grain boundary migrates, the atoms on the lattice represented by circles must move onto lattice sites associated with the orientation (represented by triangles) of the other grain. This motion occurs during grain boundary migration.

Careful examination of earlier simulations[12] allowed us to identify several distinct types of atomic motions that occur during the migration of $\Sigma5$ asymmetric tilt grain boundaries:

(i) Type I displacements (labeled I in Fig. 1) are, ideally, of zero length since these positions represent atomic sites

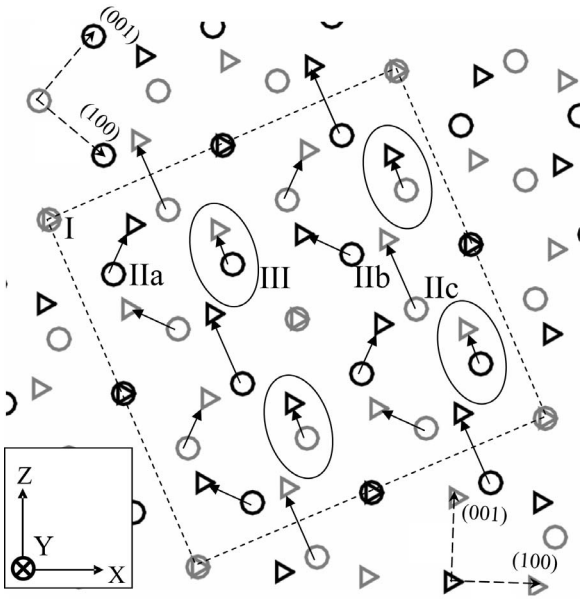

FIG. 1. Atomic jump path for an asymmetric Σ5 [010] tilt grain boundary (inclination angle α=22°). Note that the grain boundary lies in the *X*-*Y* plane of the simulation cell and orthogonal to the *X*-*Z* plane shown here. The circles and triangles represent atomic lattice sites of the crystal lattices of the two grains. The two lattices are superimposed to clarify the paths atoms follow as the boundary migrates. The dashed line represents the repeat unit cell of the superimposed lattices (i.e., it is the CSL unit cell). The unit cell extends along the *Y* axis two (010) planes. The shading of the symbols (black and gray) indicate on which (010) plane each site sits.

that are coincident in the two crystal lattices on either side of the grain boundary. These coincident sites form a regular lattice of their own—the coincident site lattice (CSL).[13]

(ii) Type II displacements (labeled IIa, IIb, and IIc in Fig. 1) are primarily in the plane perpendicular to the tilt axis (i.e., the *X*-*Z* plane in Fig. 1). These motions carry atoms across the moving grain boundary. These displacements are relatively short; less than 0.7 r_0 where r_0 is the first neighbor atomic separation in the perfect crystal.

(iii) Type III displacements (labeled III in Fig. 1) occur primarily in the boundary plane (*X*-*Y* plane in Fig. 1), and in the direction along the tilt axis (*Y* axis). These motions are a geometrically necessary component of grain boundary motion and correspond to a transformation of the local structural unit.[4] Moreover, these displacements are highly cooperative and involve the nearly simultaneous motion of several atoms in the form of a "string." On average, the strings involve 3–4 atoms under the conditions we simulate and correspond to a net jump distance of $\approx$0.8 r_0.

Previous molecular dynamics simulations[12] suggest that type II displacements are rate controlling for grain boundary migration and are triggered by localized regions of excess free volume within the grain boundary; hence grain boundary excess volume is strongly related to grain boundary mobility. We suspect that local fluctuation of free volume provides a trigger for type III displacements, but no vacancies were found at the head of the strings prior to the string motion. However, string motion is not simply a matter of particles jumping sequentially in a chain initiated by a particle hopping towards a region of high free volume. Regardless of the detailed subdynamics of this stringlike cooperative motion the motion involved ultimately results in a displacive, rather than a diffusive particle motion. Type III displacements do not produce boundary migration in themselves. Since our earlier simulations focused only on a series of Σ5 asymmetric boundaries, the generality of the observed atomistic mechanisms associated with grain boundary migration to other classes of grain boundaries remains to be demonstrated.

Although our previous investigations produced significant qualitative insights into GBM (e.g., relating the grain boundary excess volume and grain boundary mobility), several questions remained. First, what is the relationship between type II and type III displacements? The simulation results suggested that the time scale associated with the stringlike collective motion is on the order of picoseconds, while the time scale associated with type II displacements is one or two orders of magnitude larger. Second, we may reasonably ask how important the stringlike motion is for grain boundary migration. Since the stringlike motion is predominantly in the plane of the grain boundary, does it contribute to grain boundary migration in some manner? Next, we note that the results of the simulations presented in Ref. 12 were largely based upon the visualization of a series of images obtained during boundary migration and, hence, the results reported were not quantitative. The development of a boundary migration theory requires accurate, quantitative measurements. Finally, the images employed to deduce the boundary migration mechanism were obtained by quenching the simulation to T=0 K at many time intervals in order to remove thermal vibration effects. We thus implicitly assumed that GBM dynamics is not significantly changed by such quenches. It remains to be seen under what circumstances this assumption is justified.

A central feature of the earlier grain boundary simulation results[12] was the finding that stringlike, cooperative atomic motion parallel to the tilt axis, which we labeled as type III displacements. Stringlike motion of atoms has been previously observed in other contexts: grain boundary self-diffusion,[14] hard sphere melting,[15] melting in a 2-*d* plasmas,[16] and atomic dynamics in a supercooled liquids.[17–19] In particular, molecular dynamics simulations of supercooled liquids,[17–19] where the phenomenon has been studied intensively, have shown that as the temperature is lowered toward the glass transition temperature, the dynamics of supercooled liquid became "spatially heterogeneous," with regions of mobile and immobile atoms (relative to ideal Brownian motion) forming and disintegrating in dynamic equilibrium. In the mobile particle regions, stringlike cooperative motion of the atoms was observed. The average length of these strings of mobile atoms increased as the sample was cooled, and these structures have now been observed in a number of model glass-forming liquids.[17,18,20,21]

Given the existence of stringlike cooperative atomic motion in both the supercooled liquid and grain boundary migration, we utilize some of the same methods for quantifying correlated motion in these systems to analyze the molecular dynamics of grain boundary migration. This focus on quantifying the atomic motions involved in both grain boundary

dynamics and grain boundary migration requires that we avoid quenching as in our former studies. A variety of measures of "path complexity," some of which are described below, have been introduced in order to characterize the correlated nature of atom motion occurring in glass-forming liquids and other complex fluids.[22–28]

In Sec. II, we briefly discuss several statistical measures of path complexity, adapted from the liquid simulation arena, and we provide the relevant details of our simulation of GBM in the Sec. III. In Sec. IV, we focus on the dynamics of nominally stationary grain boundaries. While the stringlike (type III) cooperative atomic motion were common even in stationary boundaries, type II motions were rare. Section V focuses on the case of migrating grain boundaries. In particular, we compare the dynamics of stationary and migrating grain boundaries. Finally, we conclude with a discussion of the implication of these results for the dynamical structure of grain boundaries and grain boundary migration.

II. STATISTICAL MEASURES OF ATOMIC TRAJECTORIES AND COLLECTIVE ATOM MOTION

As in the case of supercooled liquids, the atomic motions within grain boundaries exhibit deviations from the types of atomic motions that arise in homogeneous crystals or liquids. The actual atomic motion in the grain boundaries involves a fluctuation dynamics, where localized groups of atoms in an immobile "solidlike" state coexist with atoms in a "liquidlike" state. Under these circumstances, it is natural to introduce the idealized Brownian motion of particle displacement in a fluid and Brownian motion in a harmonic potential[29] (modeling a crystal) as reference models for the atomic motions corresponding to perfectly delocalized or localized particles at long times, respectively. In both cases, the atomic motions can be naturally characterized by the self-part of the van Hove function $G_s(r,t)$, which describes the probability distribution of an atom to be displaced from its current position by an amount r after a time Δt. Mathematically, we write this "two-point function" or this self-part van Hove correlation function $G_s(r,t)$ as follows:

$$G_s(\mathbf{r},\Delta t) = \frac{1}{N}\left\langle \sum_{i=1}^{N} \delta[\mathbf{r}_i(\Delta t) - \mathbf{r}_i(0) - \mathbf{r}] \right\rangle. \tag{1}$$

For the ideal Brownian fluid, the van Hove function reduces to a simple Gaussian where the root mean square atom displacement $\langle r^2\rangle^{1/2}$ at long times is proportional to the square root of time $\Delta t^{1/2}$. For a harmonic confining potential, modeling an ideal solid, the van Hove function is also Gaussian at long times, but approaches a constant value directly related to the magnitude of the confining harmonic potential.[29] The fast inertial motions in both liquids and solids at equilibrium are governed by particle inertia and the Maxwell-Boltzmann distribution in conjunction with the ballistic nature of the trajectories in the short time regime of particle motion, regardless of whether they are in the liquid or solid states.[22]

Generally, we can expect to observe non-Gaussian behavior in a dynamical regime intermediate between the long and short time limits and where the degree of particle localization is intermediate between the idealized fluid and harmonic solid limits. By looking at G_s at different times, Δt, we can trace the path that the atom takes as it moves through the system and quantify these changes in the particle motions as the system evolves from one regime of dynamics to another. In particular, monitoring G_s during grain boundary migration will provide information on the types of displacements that the atoms are undergoing in relation to the ideal fluid and solid reference models, mentioned above. The philosophy behind this approach directly follows the philosophy of Thirumalai and Mountain[25] in the context of glass-forming liquids.

It is natural to express our observed deviations from ideally "random" atomic motion and the associated Gaussian form of G_s in terms of the Gaussian reference state. Expanding $G_s(r,t)$ in terms of Hermite polynomials[23,24] about the Gaussian distribution function (the weight function for the Hermite polynomials) reference condition naturally leads to a leading order correction term that is conventionally called the "non-Gaussian parameter," α_2. As the name implies, this parameter merely provides a measure of how much $G_s(r,t)$ deviates from a Gaussian distribution. Nonetheless, this parameter has proven to be very useful in identifying non-Brownian dynamics in glass-forming liquids and we expect that it will also prove its value in the present context. Specifically, α_2 is defined as a ratio of the second and fourth moments of the displacement distribution:

$$\alpha_2(\Delta t) = \frac{3\langle r^4(\Delta t)\rangle}{5\langle r^2(\Delta t)\rangle^2} - 1, \tag{2}$$

where $r(\Delta t)$ is the displacement of an atom in the time interval Δt. For small Δt, where inertial motions dominate, the displacements are Gaussian and thus $\alpha_2=0$. At large Δt, the atoms execute a random walk type of motion, for which the displacement distribution is also Gaussian and we again have $\alpha_2=0$ at long times. Between these limiting regimes, the behavior of $\alpha_2(\Delta t)$ exhibits evidence of the correlated motions that generally occur over intermediate times, the extent of these changes reflecting system details; a peak in α_2 at a particular Δt suggests that there is something important happening on that time scale. During grain boundary migration, the atomic motion is neither purely diffusive nor harmonic; hence, α_2 should exhibit a peak at some Δt, where fluctuation phenomena connecting these distinct evolutions result in large changes in the atom's evolution relative to Brownian motion. In this case, Δt represents a particular aspect of grain boundary migration and we may examine the trajectories in this regime to understand clearly the direct geometrical significance of this time for the atomic motions.

The dynamic entropy is another probabilistic measure of path complexity which has proven to be valuable in characterizing atomic motions in supercooled liquids. This quantity characterizes how rapidly an atom escapes its local environment. We can measure this atom escape time as a function of distance from the center of the local environment. In mathematical terms, this first passage time $\tau(R)$ required for a designated atom to cross the surface of a sphere of radius R

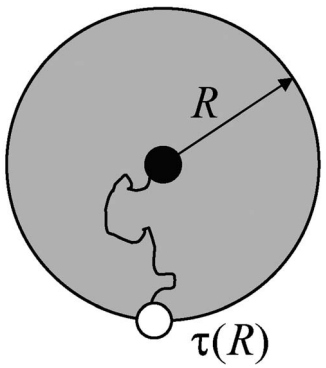

FIG. 2. Schematic illustration of the trajectory of an atom. The gray region represents the interior of a sphere of radius R. $\tau(R)$ is the time required for an atom initially at the origin to first pass through the surface of this sphere (i.e., the first-passage time).

is a measure of the inverse of the dynamic entropy S_R, as indicated in Fig. 2. The first passage term is defined as

$$\frac{1}{S_R} = \tau(R) = \int_0^\infty dt P_R(t) t \quad \text{or} \quad \tau(R) = \frac{1}{N}\sum_{i=1}^{N} \tau_i(R), \quad (3)$$

where $P_R(t)$ is the probability that an atom will first cross a sphere of radius R from its original position (at zero time) at time t, averaged over all initial times and all atoms in the system.

While the van Hove function $G_s(r,t)$ and the dynamic entropy S_R provide useful measures of the average path complexity of individual atomic motions, these measures do not address the collective nature of atomic motion that is apparent in the molecular dynamics of supercooled liquids and systems exhibiting GBM. We again draw from previous work in the field of glass-forming liquids and define a quantity called the mean string length, which is simply the average number of atoms that participate in the individual string-like collective motions that are readily apparent in visualizations of molecular dynamics trajectories. This definition identifies those atoms that have two signature properties: (i) they move an interatomic distance in times where most of the atoms have not moved an appreciable distance (i.e., they are relatively mobile), (ii) the atoms in a common string remain neighbors after the motion has occurred (e.g., all the train cars that left the station must arrive at the next stop). The mean string length, $\bar{l}(\Delta t)$ is then defined by

$$\bar{l}(\Delta t) = \frac{\sum l^2 P_l(\Delta t)}{\sum l P_l(\Delta t)}, \quad (4)$$

where $P_l(\Delta t)$ is the probability to find a string of length l in a time interval Δt. A string is defined as follows. First, identify the atoms that are mobile on the time scale Δt: we consider atoms to be mobile if the threshold condition is satisfied, $0.35r_0 < |\mathbf{r}_i(\Delta t) - \mathbf{r}_i(0)| < 0.86r_0$. The lower bound is chosen to ensure that the atomic displacement is larger than the average thermal vibration amplitude and the upper bound is chosen to ensure that the hopping distance is small compared to the atomic hop distance in the lattice and to exclude multiple atomic hops in the grain boundary. Second, mobile atoms i and j are adjacent to each other in a displacement string if $\min[|\mathbf{r}_i(\Delta t) - \mathbf{r}_j(0)|, |\mathbf{r}_i(0) - \mathbf{r}_j(\Delta t)|] < 0.43r_0$, where this bound was chosen to be less than an interatomic spacing to make sure atom i hops into the position formerly occupied by atom j (or vice versa). In order to measure the length of a string, we enumerate the list of all contiguous mobile atom pairs that satisfy this condition. While the value of the mean string length $\bar{l}$ depends on the limits we use in these criteria, any reasonable choice leads to nearly the same dependence of $\bar{l}$ on temperature, Δt, and driving force.

III. SIMULATION DETAILS AND METHODOLOGY

All of the simulations described herein were performed in three dimensions and we focus on single asymmetric $\Sigma 5$ [010] tilt grain boundaries with an inclination of $a = 22°$, where the boundary plane inclination angle, α, is measured with respect to a (103) plane in the lower crystal ($a = 0°$ is one of the two symmetric boundaries for this misorientation). The grain boundary plane normal is defined to be the Z direction and the tilt axis is along the Y direction. We can drive grain boundary migration by applying a biaxial strain $\varepsilon_{xx} = \varepsilon_{yy} = \varepsilon_0 = 2\%$. Since even the cubic material studied here (Ni) is elastically anisotropic, there is a jump in strain energy density across the boundary. The difference in strain energy density across the boundary provides the driving force for grain boundary migration. The simulation cell is periodic in the X and Y directions and the upper and lower surfaces ($\pm Z$) are free ($\sigma_{iz} = 0$). Free surfaces were employed to keep the driving force constant during boundary migration. The atomic interactions were described using the Voter-Chen[30] form of an embedded atom method (EAM)[31] potential for Ni. The simulations were performed within the canonical ensemble (NVT), where constant temperature was maintained using the Hoover-Holian[32] method at $T = 800$ K (the melting point for this model is $T_m = 1624$ K). This temperature was chosen to ensure that grain boundary migration is fast enough to be compatible with molecular dynamics time scales yet low enough that in the absence of a driving force the boundary remains relatively flat and that the natural random walk of the boundary is small. We save atomic configurations for further analysis every 0.4 ps. Further simulation details are presented elsewhere.[33,34]

IV. STATIONARY GRAIN BOUNDARY

In the absence of an applied strain ($\varepsilon_0 = 0$), the mean position of the grain boundary is stationary. During a 1.2 ns simulation, the mean position of the grain boundary does not fluctuate by more than 0.2 nm.

Figure 3 shows the mean string length, $\bar{l}(\Delta t)$, as a function of Δt at 800 K. Note that, in this calculation, we ignore strings that contain less than two atoms (the string length measures the number of atoms in the string). The mean string length increases with increasing Δt, until it reaches a maximum at $T^* \approx 80$ ps, where T^* is the value of Δt for which the string length is a maximum. It is interesting to see that even

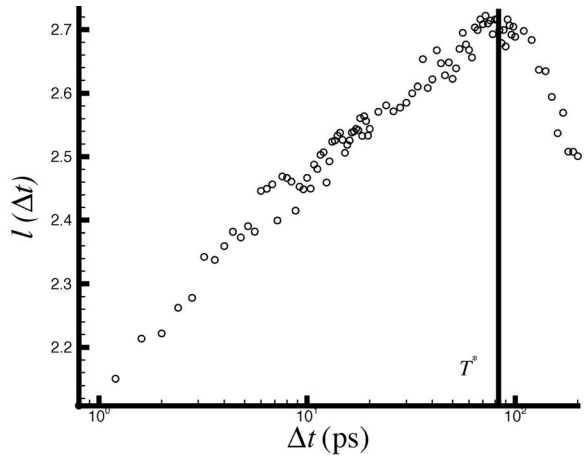

FIG. 3. The mean string length l as a function of Δt for the case of a stationary grain boundary. T^* is the time corresponding to the maximum mean string length.

when the grain boundary is not migrating, stringlike cooperative motion occurs within the grain boundary, as it does in glass-forming liquids. At small Δt, the atomic motion simply involves the inertial motion of individual atoms. In the limit of large Δt, atomic motion is uncorrelated; the long time motion of individual atoms appears to be Brownian. Between these extremes, there is an intermediate time scale $\Delta t = T^*$ where correlated atom motion becomes highly developed and the string-length becomes maximal. Since stringlike cooperative motion occurs in the absence of a driving force, we must conclude that the cooperative motion is an intrinsic part of the (clusterlike) internal dynamics of grain boundaries.

Figure 4 shows all of the atoms that are members of strings $\bar{l} > 4$ at $\Delta t = T^*$ in a boundary plane (X-Y) view during the entire 1.2 ns simulation. This figure clearly shows that the strings predominantly form in the direction parallel to the tilt axis in a regular set of lines. While such linear strings always appear parallel to the tilt axis as we vary the boundary inclination, the spacing between them depends on boundary inclination. These linear strings are the type III displacements observed previously[12] and correspond to the motion labeled III in Fig. 1 (i.e., with displacements primarily along the tilt axis). Since the grain boundary is essentially stationary during the course of these simulations, the stringlike atomic motion parallel to the tilt axis does not directly couple to the translation of the grain boundary. Rather, in this case, the strings move atoms back and forth along the tilt axis direction, Y. Within the train dynamics analogy, this is like the rocking inertial dynamics motions of a long train as it starts to move from a stopped state.

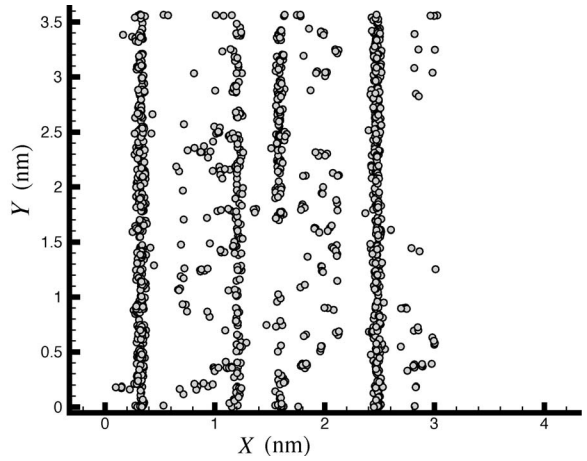

FIG. 4. Identification of all of the atoms that are members of strings of length greater than four at $\Delta t = T^*$ in a boundary plane (X-Y) view during the entire simulation.

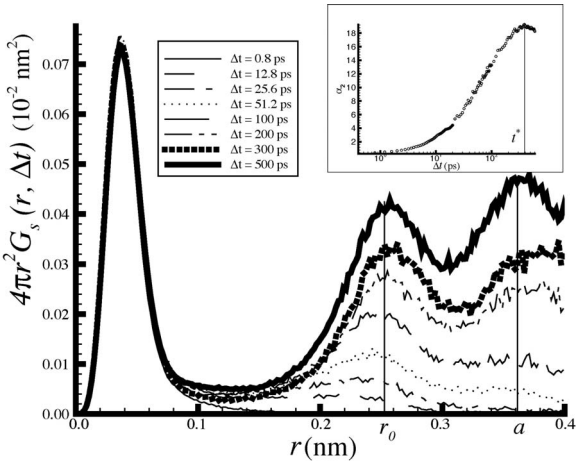

FIG. 5. The displacement distribution function G_s at eight different Δt for the case of a stationary boundary. The inset shows the non-Gaussian parameter α_2 as a function of Δt. The time t^* corresponds to the maximum in α_2.

The van Hove function $G_s(r, \Delta t)$ is shown in Fig. 5 for eight different values of Δt. At small Δt (<0.8 ps), the G_s is nearly Gaussian as is appropriate for inertial or harmonically localized motion. The inset in this figure shows the non-Gaussian parameter, α_2, versus Δt. We see that at $\Delta t = 0.8$ ps, this parameter is nearly zero—confirming the Gaussian nature of the atomic motion on this time scale. The displacement r corresponding to the single peak observed at $\Delta t = 0.8$ ps is a measure of the vibration amplitude of the atoms at this time scale. As Δt increases, the G_s begins to show deviations from the Gaussian distribution. In particular, a second peak is discernable by $\Delta t \approx 25.6$ ps. With further increase in Δt, this second peak position becomes fixed at $r = r_0$, which is the position of the first nearest-neighbor distance in a defect-free crystal lattice. With increasing Δt (beyond $\Delta t \approx 51.2$ ps), we observe a third peak forming in the distribution function. The position of this peak corresponds to the second nearest-neighbor distance in the perfect face centered cubic lattice, i.e., the cubic lattice parameter, a. At large times $\alpha_2(\Delta t)$ continues to grow in magnitude, reaching a peak at $\Delta t = t^*$. In the present case, this maximum occurs at $t^* \sim 400$ ps. It is interesting to note that this time scale, t^*, is approximately five times larger than the time scale associated with the stringlike cooperative motion T^* (≈ 80 ps). This implies that, for grain boundary motion, this non-Gaussian behavior represents different types of atomic dynamics than the stringlike motion, discussed earlier.

Examination of Fig. 5 shows that there is no peak in the G_s at the distance corresponding to motion III in Fig. 1,

which we associated with the type III stringlike cooperative motion. If such a peak was present, it would be at $r=0.2$ nm. This is not surprising since for large Δt ($\Delta t \gg T^*$) the back-and-forth nature of the stringlike motion would wash out the displacements; i.e., the net displacement would be nearly zero. However, if we look on time scales comparable with T^*, we should expect to find stringlike displacements. Examining G_s in Fig. 5 around the motion III distance, $r=0.2$ nm, we see no weight at $\Delta t=0.8$ ps, but we do see weight developing and growing there in the $\Delta t=12.8$, 25.6, 51.2, and 100 ps curves, before it saturates. This is the time regime where the string length is appreciable. This suggests that the weight we see in the G_s around 0.2 nm is a signature of the stringlike motion that we observe in simulations. This is supported by the fact that the second peak in G_s does not simply grow in amplitude with increasing Δt, but rather grows and shifts towards larger r as the true second peak at r_0 superimposes with the small stringlike motion peak that occurs at ≈ 0.2 nm. It is also worth noting that the stringlike motion "peak" is small because the strings are relatively short.

We note that we do not see a peak in Fig. 5 at distances corresponding to the atomic motions IIa, IIb, and IIc in Fig. 1 (these should be at 0.11, 0.11, and 0.16 nm, respectively). However, this is not surprising since these displacements are associated with boundary migration (they have a large projection normal to the boundary plane) and essentially no boundary migration occurs here (low T, no driving force for migration). Nonetheless, an examination of the non-Gaussian parameter, $\alpha_2(\Delta t)$, shown in the inset to Fig. 5 shows that whatever the cause of the peak at 400 ps, it appears to have little effect on the $G_s(r,t)$. If such motions are type II displacements, sufficiently few atoms are involved in such motion in this stationary boundary situation to have a significant effect. Yet, it may be that these motions at 0.11 and 0.16 nm contribute to the broadness of the very small stringlike motion peak, but they get "washed out" as the peak at r_0 grows.

The second peak in the G_s in Fig. 5 occurs at $r=r_0$, which does not correspond to any of the displacements seen in Fig. 1. We now examine the origin of this peak with the use of Fig. 6, which shows atomic trajectories at or near the grain boundary. In this figure, each displacement vector corresponds to a 0.8 ps time step, with the lighter lines (blue in the online version) correspond to the earliest times and the darker lines (red) to late times. The black and white circles represent the perfect crystal lattice sites of the lower and upper crystals, respectively. This figure suggests that most of the atoms simply vibrate around fixed lattice sites (these are responsible for the first peak in the G_s in Fig. 5). There is a small band, parallel to the X axis ($9.6\ \text{nm} \leqslant Z \leqslant 10.0$ nm) in Fig. 6, where we see displacements of atoms from one lattice site to another—white-to-white, white-to-black, etc. These displacements occur at the boundary and are part of the intrinsic dynamics of the boundary. Type III displacements (i.e., stringlike displacements occur primarily in the Y direction) occur in the regions indicated by the large circles. Such displacements correspond to atoms jumping from the white-to-black lattice sites within the circle (and a large motion in the Y direction). The black arrows in the figure correspond to displacements of length r_0. These displacements occur between atomic sites in the string and adjacent atomic sites. It is these motions that create the second peak in the G_s. Therefore, while the type III motions are primarily responsible for atomic motion in the Y direction (parallel to the tilt axis) on a very short time scale, atoms escaping from the string give rise to the strong peak in G_s at r_0. These motions correspond to atomic jumps from one lattice site to a neighboring lattice site in the same crystal. However, this does not appear to be normal vacancy diffusion, since such jumps only occur at the grain boundary and the vacancy concentration at the grain boundary is nearly zero in these low temperature simulations.

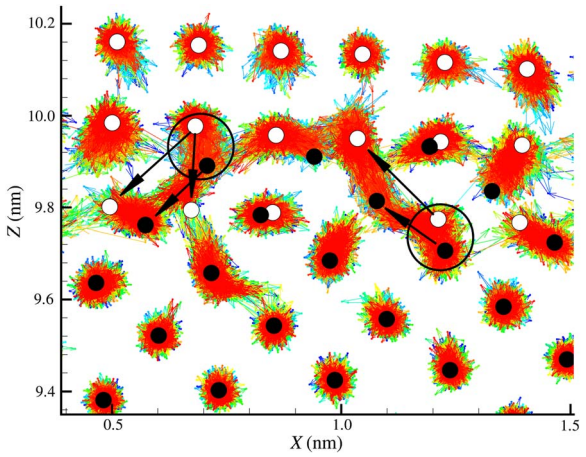

FIG. 6. (Color online) The atomic trajectories at/near the grain boundary. Displacement vectors are shown every 0.8 ps. The lighter lines (blue in the online version) correspond to early times and the darker lines (red) to late times. The black and white circles represent the perfect crystal lattice sites of the lower and upper crystals, respectively. Type III displacements are predominantly in the direction perpendicular to the plane shown, but occur at locations indicated by the two large circles. The black arrows indicate translation vectors of length r_0.

The third peak in the G_s in Fig. 5 occurs at $r=a$, where a takes the value for the perfect crystal lattice parameter. Such a displacement may be associated with two atomic hops of the same atom along one of the strings, parallel to the tilt axis within time Δt.

V. MIGRATING GRAIN BOUNDARY

In this section, we examine the same grain boundary as in the previous section of this paper, but now we consider the case where the boundary migrates under the driving force associated with an applied biaxial strain. In the present simulations, the applied strain was 2% (in both the X and Y directions) and the grain boundary migrates (in the Z direction) by 2.5 nm in 0.9 ns (the face centered cubic lattice parameter is 0.35 nm).

Figure 7 shows the mean string length as a function of Δt for the cases of the migrating and stationary grain boundary. The variation of the mean string length with Δt is similar in the two cases. While the two curves are identical for short time, the maximum mean string length occurs at smaller Δt for the migrating grain boundary than for the stationary one;

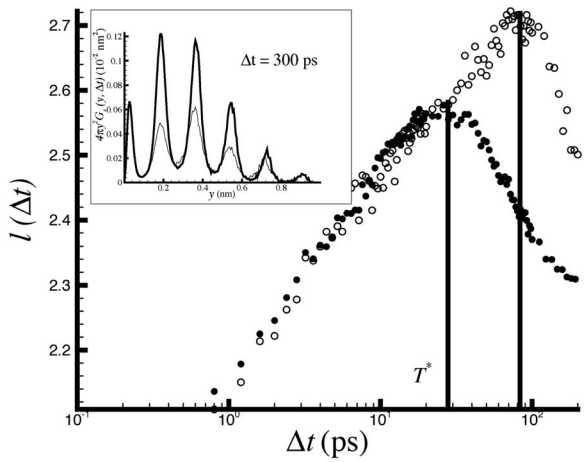

FIG. 7. The mean string length as a function of Δt for a migrating boundary (the stationary boundary results are repeated here for comparison). The filled (open) circles indicate data for the migrating (stationary) boundary. The inset shows the Y component of displacement distribution function for both cases. The dark (light) line denotes the migrating (stationary) boundary.

i.e., $T^*=80$ ps in the stationary case and $T^*=26$ ps in the case of the migrating boundary. While this figure shows that stringlike displacements occur in the migrating boundary, a plot of G_s in the tilt axis direction (Y) that is shown in the inset suggests that the atomic motions in this direction are discrete. Each of the individual jumps is of length equal to the distance between two (010) planes (one half of the lattice parameter). Comparison of G_s for the migrating and stationary boundary (both shown in the inset) demonstrates that the stringlike motion is much more intense when the boundary migrates. Therefore, although the mean string length is larger in the stationary boundary than the moving boundary, the number of atoms involved in stringlike motion is actually larger in the migrating boundary case.

Figure 8 shows all of the atoms that are part of strings of length greater than four atoms at $\Delta t=T^*$ in the transboundary plane (X-Z) view during the entire 0.9 ns simulation. We circled those locations where many such atoms appear to be clustered. It is not surprising to find that it is these positions that correspond to motion III (type III displacements) in Fig. 1. This again confirms that type III displacements are associated with stringlike cooperative motion.

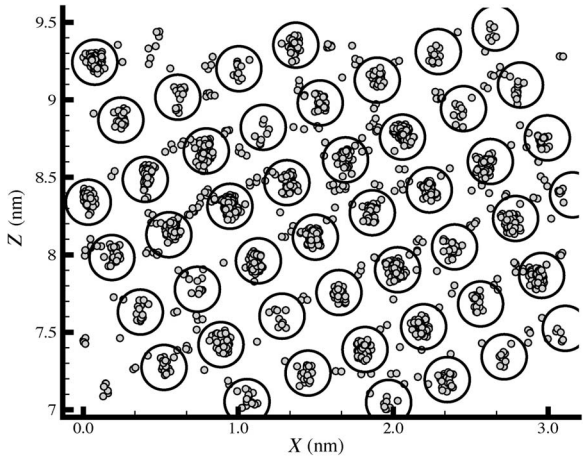

FIG. 8. The position of atoms in strings of length greater than four at $\Delta t=T^*$ in a transboundary plane (X-Z) view during the entire simulation. Circles denote the places where Type III displacements occur (predominantly perpendicular to the plane of this image).

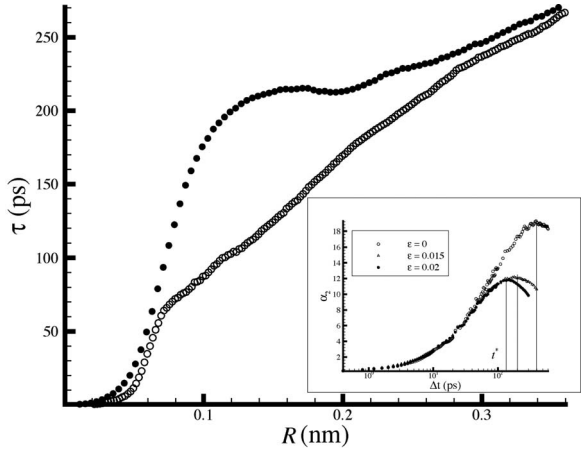

FIG. 9. A comparison of the mean first-passage time as a function of R for both the stationary (open circle) and migrating boundaries (filled circle). The inset shows the non-Gaussian parameter α_2 as a function of Δt for the same cases (at $\varepsilon=0\%$, 1.5%, and 2%).

Figure 9 shows the mean first-passage time τ as a function of jump distance R for both stationary and migrating boundaries. The behavior of $\tau(R)$ is nearly identical in the two cases at small R. This is presumably associated with the nearly harmonic motion of the atoms for small R. For large R, both curves become nearly linear (crossing at larger R than shown here). We note, however, that very few atoms reach large jump distances in the migrating boundary case since as the boundary migrates the individual atoms are left behind within the crystal and, hence, only move as dictated by the (small) bulk diffusivity. There is a transition region between the short time inertial motion and a linear $\tau(R)$ behavior at large R corresponding to ballistic motion. This region is relatively small in the stationary grain boundary case (between 0.05 and 0.07 nm), but much more extended in the migrating boundary case (0.05 and 0.1 nm). In the transition region, $\tau(R)$ is approximately an exponential function.

We now focus on $\tau(R)$ for the migrating boundary in more detail. Examination of Fig. 5 (and the inset to Fig. 7) shows that the first peak in G_s is at approximately 0.05 nm. This is associated with atom vibrations around their lattice sites. It is these vibrations that are responsible for the behavior of $\tau(R)$ at distances of 0.05 nm and less. The fact that $\tau(R)$ rises exponentially with R in the beginning of the transition region suggests that this atomic motion corresponds to escape from a local cage (this is probably thermally activated). The cage size can be determined from the inflection of the curve in the transition region. This inflection corresponds to a cage size of $r=0.08$ nm and an average escape time of ≈ 130 ps.

The inset in Fig. 9 shows the non-Gaussian parameter α_2 versus Δt for both the stationary and migrating boundaries. As for the mean first-passage time τ, the non-Gaussian parameter also shows a maximum around 130 ps. This suggests

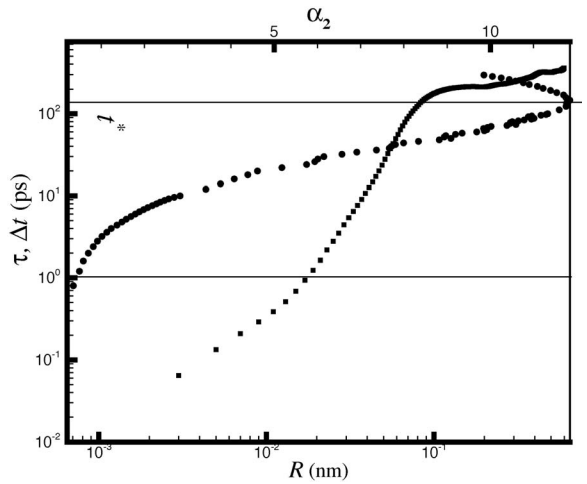

FIG. 10. A comparison of the mean first-passage time (filled square) and non-Gaussian parameter (filled circle) versus time for the migrating grain boundary.

that the characteristic time associated with the transition in the mean first-passage time and the time corresponding to the maximum in the non-Gaussian parameter α_2 are related. This can be seen clearly in Fig. 10 where we plot α_2 vs Δt and τ vs R on the same plot for the migrating boundary case. For time <1.0 ps, the atomic motion is harmonic (i.e., α_2 is nearly zero) and R is a linear function of time. At the time t^* (≈ 130 ps), α_2 is a maximum and there is a relatively abrupt change in the mean first-passage time vs R. This suggests that both of these quantities provide different views of the same types of events that occur during boundary migration. These events are, however, not the stringlike cooperative motions that occur on short time scales ($26\ \text{ps} = T^* \ll t^* = 130$ ps).

In order to better understand the type of event occurring on the time scale of t^*, we investigate G_s as function of Δt, as shown in Fig. 11. For $\Delta t < t^*$, G_s for the migrating and stationary boundaries are very similar. That is, for $\Delta t \approx 0.8$ ps G_s is approximately Gaussian, and a second peak appears at $r = r_0$ at $\Delta t \approx 50$ ps and a third appears at $r = a$ at Δt

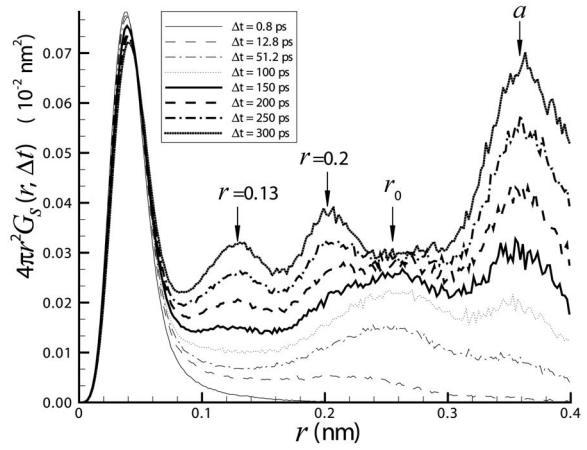

FIG. 11. The displacement distribution function G_s at eight different time intervals Δt for the migrating grain boundary.

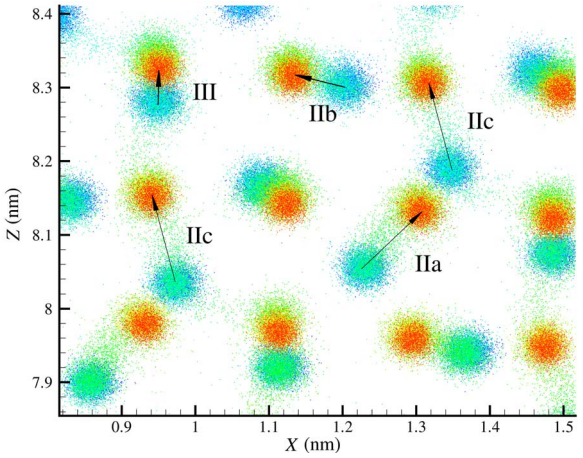

FIG. 12. (Color online) Transboundary plane view (X-Z) of the atom positions (individual dots) every 0.8 ps for 1000 time intervals.

≈ 100 ps. However, for $\Delta t > t^*$, G_s for the stationary and migrating boundaries show very different features. In other words, the displacement distribution function for the migrating boundary develops new peaks at $r=0.13$ and $r=0.2$ nm and the peak at r_0 begins to disappear (or at least stops growing). These observations suggest that the atomic events that begin on the time scale t^* are associated with atomic displacements of length 0.13 and 0.2 nm.

Figure 12 shows a transboundary plane view (X-Z) of the bicrystal, showing that atomic arrangement of the system at 1000 intervals, 0.8 ps apart. In this image the early time positions are shown in light gray (blue in the online version) and the late time position in black (red online). Since the image shows the position of each atom at 1000 times, it can be viewed as a multiple exposure image. As such, this image provides information on how individual atoms move from their locations in one crystal to their new locations in the other crystal as the grain boundary passes (the grain boundary has traversed the entire system shown in the figure). Examination of Fig. 12 shows that the average atomic displacements for motions IIa, IIb, and IIc (type II displacements) are 0.113, 0.071, and 0.124 nm, respectively, while the average hopping distance for motion III (type III displacement) is 0.195 nm (this is mostly in the direction orthogonal to the plane shown here). Based on this, we can conclude that the broad peak at $r=0.13$ nm in G_s (Fig. 11) represents type II displacements (motions IIa and IIc), and the peak of $r=0.2$ nm represents type III displacement (motion III).

These observations confirm the assertion that it is the type II displacements that are associated with the boundary migration process and that these displacements control the rate of boundary migration. At time shorter than t^*, the atomic structure of the grain boundary is dynamic, but is waiting for a fluctuation of the requisite amplitude to develop that will result in a type II displacement event. The short time dynamics is dominated by stringlike displacement cascades that involve atomic displacement of ≈ 0.2 nm. These displacements correspond to the motion of the strings both back and forth. Interestingly, at times longer than t^*, the type III, stringlike atomic motions are biased such that each string moves more

in one direction than back. This is why the peak in G_s at $r=0.2$ nm becomes pronounced for times longer than t^*. We can now also understand why the peak in the displacement distribution function G_s at $r=r_0$ disappears at times longer than t^*. We recall that this peak, which was prominent in the stationary boundary case, corresponds to compound atomic hops—(i) along a string and then (ii) off the string but into a lattice position of the original crystal. When the boundary migrates, the target lattice position for the second hop is gone because the boundary has replaced the original crystal with that of the grain on the other side of the boundary.

VI. DISCUSSION AND CONCLUSION

The main focus of this paper is identifying the types and nature of the atomic motions that occur in both a stationary and migrating grain boundary ($\Sigma5$ [010] asymmetric grain boundary) using molecular dynamics simulations at 800 K. A particularly striking feature of these atomic dynamics is a cooperative motion of string of atoms, in the direction parallel to the tilt axis.[12] Interestingly, similar stringlike cooperative motions of atoms were observed in supercooled liquids.[17] Because of the similarities between the stringlike motions observed both in grain boundaries and liquids, we focused, in this paper, on the application of the statistical tools used for analyzing atomic dynamics in liquids. This approach allows us to directly study the atomic dynamics as they occur, without quenching to 0 K (as in previous work[12]) and to observe the relevant dynamics in a statistically meaningful manner.

In our earlier study of the atomic dynamics during boundary migration,[12] we identified this stringlike cooperative motion (type III displacements) as a key feature of grain boundary migration. The present work demonstrates that such stringlike motion is a regular feature of the atomic dynamics whether the boundary is migrating or is stationary. This suggests that stringlike cooperative motion is indeed an intrinsic feature of grain boundary dynamics and may contribute to diffusion in the boundary plane (and all of the properties affected by grain boundary diffusion, such as nucleation and growth of new phases, solute transport, stress relaxation, Coble creep, and grain boundary sliding). The presence of stringlike motion was previously reported in a simulation study of self-diffusion in $\Sigma5$ symmetric grain boundaries[14] (although in this study, stringlike motion was found to occur primarily in the direction perpendicular to the tilt axis). While we expect stringlike cooperative motion to be a general property of grain boundary dynamics, whether this motion occurs primarily parallel to the tilt axis may not be completely general; it will undoubtedly depend on the overall boundary structure. Nonetheless, the tilt axis is a key determinate of that structure and will remain special. In the absence of a driving force, the (predominantly linear) strings move back-and-forth along the tilt axis. In this case, the motion of the individual strings is unbiased and leads to no net grain boundary migration. As shown in Fig. 3, the characteristic time scale T^* associated with stringlike motion in the stationary boundary is $\approx$80 ps. Curiously, this time drops to $\approx$26 ps (see Fig. 7) when we apply a strain ($\varepsilon_0=2\%$) to force the boundary to migrate. In the migrating boundary, the average length of the string is also substantially reduced. Clearly, the applied driving force tends to decorrelate this type of cooperative motion. Since the stringlike cooperative motion (type III events) occurs on a much shorter time scale than other important dynamic events in boundary migration (type II events), stringlike motion is not rate controlling. Therefore, the change in the atomic dynamics on the application of the driving force for boundary migration has little effect on the net grain boundary migration rate. Note, that while the mean square displacement associated with type III events is close to 0.2 nm, the net displacement related to type III events is close to zero since the probability for a string to travel along the $\pm Y$ directions (tilt axis) are equal, therefore no tangential migration along tilt axis will be induced by type III displacements.

The types of atomic displacements that are referred to as type II events in this paper correspond to atomic motion across the boundary plane (recall type III events are predominantly in the plane). To more completely characterize type II events, we employ several path complexity measures: the non-Gaussian parameter, the mean first-passage time, and displacement distribution function. The characteristic time scale for type II displacements is $t^*\approx130$ ps. This time scale corresponds to the maximum value of the non-Gaussian parameter and an abrupt change in the first-passage time (see Fig. 10). In addition, this time corresponds to important changes in the form of the displacement distribution function (see Fig. 11). Clearly, type II events occur over a much longer time scale than do the stringlike type III events and it is likely that this type of event controls the rate at which boundaries migrate.

As discussed above, it is the type II events that carry the boundary forward—they correspond to atomic jumps from the crystal lattice of one grain to that of the other. In the absence of a driving force for migration, these jumps still occur. However, in this case, they go, at equal rates, back and forth—leading to no net boundary migration (apart from a random walk). When a driving force is applied, the direction of these events is biased, leading to net migration. In the absence of a driving force, the characteristic time associated with type II events is $t^*\approx400$ ps, rather than the $t^*\approx130$ ps observed when a 2% strain is used to drive the boundary migration (see the inset to Fig. 9). This difference is indicative of the change from the random walk of the boundary to an applied force driven type of boundary migration. In other words, it represents the change from the back-and-forth hops between the two crystal lattices to a directed atomic hop mechanism from one lattice to the other at the boundary. In real grain boundaries, the type II events may occur preferentially near secondary grain boundary dislocations or other defects in the boundary structure.

Since we found that the driving force biases the type II atomic hopping, it is interesting to inquire as to whether the driving force also biases the directed type III atomic motions. The displacement distribution function (Fig. 11) provides an answer to this. It shows that a new peak (near 0.2 nm) forms on the time scale associated with driven boundary migration (i.e., 130 ps). The position of this peak corresponds to the jump distance within a string. In the ab-

sence of a driving force, we see no net displacement accompanying stringlike motion, since the strings move back-and-forth. However, once the boundary begins to migrate, the atoms in the strings are biased to move more in one direction than the other (more forth and less back).

In summary, we find that the two most important classes of atomic dynamics in grain boundaries are a stringlike motion in the boundary plane (type III) and atomic motions that are predominantly out of plane that lead to boundary migration (type II). Type III events imply that the atomic motion are collective as observed or suggested by a number of other works,[5,7,10,11,14] while type II events imply that such atomic motions are controlled by the single atom hops mechanism as suggested in Refs. 8 and 9. The characteristic time associated with type II events occur on a significantly longer time scale than that for type III events (130 ps versus 26 ps at the strain and temperature considered here). The application of a driving force for boundary migration affects both of these events. It shortens string lengths and the time scale for type III events (from 80 to 26 ps). It shortens the characteristic time for type II events from 400 to 130 ps. Since type II events necessarily lead to boundary translation, the rate at which these events occur controls the rate of boundary migration. While type III events may be necessary to redistribute free volume to allow for type II events, these occur on a much shorter time scale and hence do not limit the rate of boundary migration.

ACKNOWLEDGMENTS

The authors gratefully acknowledge the support of the U.S. Department of Energy, through Grant No. DE-FG02-99ER45797, the National Institute of Standards and Technology, and the Computational Materials Science Network.

[1] M. F. Ashby, Surf. Sci. **31**, 498 (1972).
[2] G. H. Bishop, R. J. Harrison, T. Kwok, and S. Yip, J. Appl. Phys. **53**, 5596 (1982).
[3] J. W. Cahn and J. E. Taylor, Acta Mater. **52**, 4887 (2004).
[4] A. Suzuki and Y. Mishin, Mater. Sci. Forum **502**, 157 (2005).
[5] N. F. Mott, P. Phys. Soc. Lond **60**, 391 (1948).
[6] S. E. Babcock and R. W. Balluffi, Acta Metall. Mater. **37**, 2357 (1989).
[7] S. E. Babcock and R. W. Balluffi, Acta Metall. Mater. **37**, 2367 (1989).
[8] H. Gleiter, Acta Metall. Mater. **17**, 853 (1969).
[9] H. Gleiter, Acta Metall. Mater. **17**, 565 (1969).
[10] R. J. Jhan and P. D. Bristowe, Scr. Metall. Mater. **24**, 1313 (1990).
[11] B. Schonfelder, D. Wolf, S. R. Phillpot, and M. Furtkamp, Interface Sci. **5**, 245 (1997).
[12] H. Zhang and D. J. Srolovitz, Acta Mater. **54**, 623 (2006).
[13] A. P. Sutton and R. W. Balluffi, *Interfaces in Crystalline Materials* (Clarendon Press, Oxford, 1995).
[14] M. R. Sorensen, Y. Mishin, and A. F. Voter, Phys. Rev. B **62**, 3658 (2000).
[15] B. J. Alder, W. G. Hoover, and T. E. Wainwright, Phys. Rev. Lett. **11**, 241 (1963).
[16] P. Choquard and J. Clerouin, Phys. Rev. Lett. **50**, 2086 (1983).
[17] C. Donati, J. F. Douglas, W. Kob, S. J. Plimpton, P. H. Poole, and S. C. Glotzer, Phys. Rev. Lett. **80**, 2338 (1998).
[18] Y. Gebremichael, T. B. Schroder, F. W. Starr, and S. C. Glotzer, Phys. Rev. E **64**, 051503 (2001).
[19] Y. Gebremichael, M. Vogel, and S. C. Glotzer, J. Chem. Phys. **120**, 4415 (2004).
[20] Y. Gebremichael, M. Vogel, M. N. J. Bergroth, F. W. Starr, and S. C. Glotzer, J. Phys. Chem. B **109**, 15068 (2005).
[21] N. Giovambattista, S. V. Buldyrev, H. E. Stanley, and F. W. Starr, Phys. Rev. E **72**, 011202 (2005).
[22] P. Allegrini, J. F. Douglas, and S. C. Glotzer, Phys. Rev. E **60**, 5714 (1999).
[23] A. Rahman, J. Chem. Phys. **45**, 2585 (1966).
[24] A. Rahman, Phys. Rev. A **136**, A405 (1964).
[25] D. Thirumalai and R. D. Mountain, Phys. Rev. E **47**, 479 (1993).
[26] A. I. Melcuk, R. A. Ramos, H. Gould, W. Klein, and R. D. Mountain, Phys. Rev. Lett. **75**, 2522 (1995).
[27] P. Gaspard and X. J. Wang, Phys. Rep. **235**, 291 (1993).
[28] P. Gaspard, Adv. Chem. Phys. **99**, 369 (1997).
[29] M. Doi and S. F. Edwards, J. Chem. Soc., Faraday Trans. 1 **74**, 1789 (1978).
[30] A. F. Voter and S. P. Chen, in *Accurate Interatomic Potentials for Ni, Al and Ni3Al*, edited by R. W. Siegel, J. R. Weertman, and R. Sinclair, MRS Symposia Proceedings No. 82 (Materials Research Society, Pittsburgh, 1987), p. 175.
[31] S. M. Foiles, M. I. Baskes, and M. S. Daw, Phys. Rev. B **33**, 7983 (1986).
[32] W. G. Hoover and B. L. Holian, Phys. Lett. A **211**, 253 (1996).
[33] H. Zhang, M. I. Mendelev, and D. J. Srolovitz, Scr. Mater. **52**, 1193 (2005).
[34] H. Zhang, M. I. Mendelev, and D. J. Srolovitz, Acta Mater. **52**, 2569 (2004).